Pressure tuning of structural and magnetic transitions in $EuAg_4As_2$

Sergey L. Bud'ko,[1,*] Li Xiang,[1] Chaowei Hu,[2] Bing Shen,[2] Ni Ni,[2] and Paul C. Canfield[1]

[1]*Ames Laboratory, U.S. Department of Energy, and Department of Physics and Astronomy, Iowa State University, Ames, Iowa 50011, USA*

[2]*Department of Physics and Astronomy and California NanoSystems Institute, University of California, Los Angeles, Los Angeles, California 90095, USA*

(Received 28 January 2020; revised manuscript received 10 April 2020; accepted 21 April 2020; published 7 May 2020)

We report temperature-dependent measurements of ambient-pressure specific heat, magnetic susceptibility, anisotropic resistivity, and thermal expansion as well as in-plane resistivity under pressure up to 20.8 kbar on single crystals of $EuAg_4As_2$. Based on thermal expansion and in-plane electrical transport measurements at ambient pressure this compound has two, first-order, structural transitions in the 80–120 K temperature range. Ambient-pressure specific heat, magnetization, and thermal expansion measurements show a cascade of up to seven transitions between 8 and 16 K associated with the ordering of the Eu^{2+} moments. In-plane electrical transport is able to detect the more prominent of these transitions, at 15.5, 9.9, and 8.7 K, as well as a weak feature at 11.8 K at ambient pressure. Pressure-dependent electrical transport data show that the magnetic transitions shift to higher temperatures under pressure, as does the upper structural transition, whereas the lower structural transition is suppressed and ultimately vanishes. A jump in resistivity, associated with the upper structural transition, decreases under pressure with an extrapolated disappearance (or a change of sign) by 30–35 kbar. In the 10–15 kbar range a kink in the pressure dependency of the upper structural transition temperature as well as the high- and low-temperature in-plane resistivities suggests that a change in the electronic structure may occur in this pressure range. The results are compared with the literature data for $SrAg_4As_2$.

DOI: 10.1103/PhysRevB.101.195112

I. INTRODUCTION

Since the discovery of high-temperature superconductivity in iron-arsenides [1,2], studies of the physical properties of large families of pnictide-based compounds have attracted a lot of attention. The interplay between different orders, such as the coexistence, competition, and/or correlation of superconductivity, magnetism, and structural phase transitions (or nematicity) in pnictides [3–6], has made these families a playground for condensed matter physicists, chemists, and materials scientists. Europium-based pnictides occupy a special position in the family since they add local, Eu^{2+} magnetism to the complexity of the observed orders [5].

The new, trigonal, layered arsenide, $EuAg_4As_2$, and its nonmagnetic counterpart, $SrAg_4As_2$, were first synthesized a few years ago [7]. In polycrystalline samples of $EuAg_4As_2$ the divalent nature of europium and the antiferromagnetic order at $T_N = 14.9$ K were determined from magnetization and ^{151}Eu Mössbauer measurements [8]. More recently, detailed structural, thermodynamic, and transport studies of single crystals of $EuAg_4As_2$ revealed a complex physical picture that includes a structural distortion at 120 K and incommensurate, noncollinear long-range antiferromagnetism developing at 9 K [9]. The magnetic transition at ∼15 K [8], based on detailed recent ^{151}Eu Mössbauer data [10], was suggested to be a transition from a paramagnetic state to an incommensurate sine-modulated long-range order. A detailed, ambient-pressure, single-crystal x-ray diffraction study was performed [9] between room temperature and 100 K. At room temperature the crystal structure of $EuAg_4As_2$ was found to correspond to the $R\bar{3}m$ (No. 166) space group, as described in the literature [7]. At 100 K satellite peaks corresponding to two propagation vectors, $q_1 = \pm(0, 0.25, 0.5)$ and $q_2 = \pm(0.25, 0, 1)$, were reported to appear, suggesting the existence of a structural distortion at low temperatures. Motivated by the complexity and interplay of different orders in $EuAg_4As_2$ as well as reported curious, nonmonotonic pressure dependence of the structural transition in its nonmagnetic analog, $SrAg_4As_2$ [11], in this work we study the tunability of magnetic and structural transitions in $EuAg_4As_2$ by hydrostatic pressure via in-plane resistivity measurements.

II. EXPERIMENTAL DETAILS

Single crystals of $EuAg_4As_2$ were grown out of a high-temperature melt with an excess of Ag_2As. Details of the synthesis can be found elsewhere [9]. Resulting platelike single crystals (c axis perpendicular to the plates) were of several millimeter in-plane dimensions and over a millimeter thick. In order to allow ambient-pressure comparison, a detailed set of ambient-pressure measurements was done on the particular batch of crystals that was later used for transport measurements under pressure. Ambient pressure, in-plane and c-axis, ac ($f = 16$ Hz) resistivity measurements were performed in a standard, linear, four-probe configuration using an ACT option of a Quantum Design Physical Property Measurement System (PPMS). Electrical contacts to the

*budko@ameslab.gov

sample were made using Epotek H20 silver epoxy. Magnetization measurements were performed in a Quantum Design MPMS3 magnetometer. Low-temperature heat capacity measurements were made using semiadiabatic thermal relaxation technique as implemented in the heat capacity option of the Quantum Design PPMS. Anisotropic thermal expansion measurements were carried out using an OFCH copper capacitive dilatometer [12].

In-plane resistivity measurements under pressure were performed in a hybrid, Be-Cu/Ni-Cr-Al piston-cylinder pressure cell (modified version of the one used in Ref. [13]) in the temperature environment provided by a PPMS instrument. A 40:60 mixture of light mineral oil and *n*-pentane was used as a pressure-transmitting medium. This medium solidifies at room temperature in the pressure range of 30–40 kbar [13–15], which is above the maximum pressure in this work. Elemental Pb was used as a low-temperature pressure gauge [16]. The measurements were performed both on an increase and on a decrease in pressure and the results are reversible. It has been known [17–21] that in piston-cylinder pressure cells high-temperature pressures are different from low-temperature pressures and the temperature dependence of this pressure difference is nontrivial. Given that the temperature/pressure relation for this specific cell/pressure medium combination has not been established, here we simply use the Pb gauge pressure value. This may give rise to pressure differences, at higher temperatures, of up to 3 kbar.

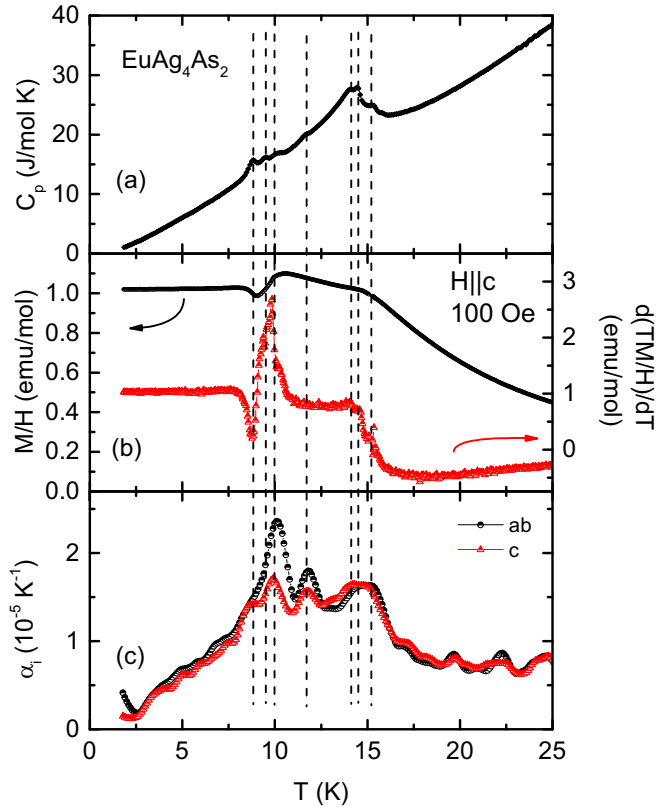

FIG. 1. Low-temperature part of (a) the heat capacity, (b) the magnetic susceptibility, M/H, measured in a magnetic field $H =$ 100 Oe applied parallel to the c axis, and the temperature derivative, $d(T\,M/H)/dT$ [22], and (c) the anisotropic thermal expansion coefficients, α_i. Heat capacity data were taken on cooling; magnetization and thermal expansion data, on warming. Vertical lines mark transitions as seen in the low-temperature heat capacity.

III. RESULTS

A. Ambient pressure

Low-temperature heat capacity data are shown in Fig. 1(a). The data are complex and suggest that up to seven transitions (shown by dashed vertical lines) occur in $EuAg_4As_2$ below 16 K as the Eu^{2+} moments order. The low-temperature, low-field magnetic susceptibility, M/H, and its derivative in the form of $d(TM/H)/dT$ [22] have anomalies at similar temperatures [Fig. 1(b)], although the one at ~11.8 K is not discernible, at least for $H \| c$. This identification of possible transition temperatures shows a fair agreement with the anisotropic thermal expansion data shown in Fig. 1(c). Altogether, three different thermodynamic measurements indicate as many as seven, closely spaced low-temperature transitions. This density of transitions is remarkable but not unprecedented; CeSb has seven transitions between 8 and 18 K in zero applied magnetic field and an even larger number of additional transitions in applied fields [23].

Anisotropic thermal expansion (Fig. 2) serves as a thermodynamic probe of the phase transitions (the structural ones, in particular). Indeed, both structural phase transitions are clearly seen in the thermal expansion $[L_i(T) - L_i(1.8\ \mathrm{K})/L_i(1.8\ \mathrm{K})$ data, where L_i is the sample's length, either along the c axis or in the ab plane. Whereas the lattice change is large and in the same direction for both lattice parameters at the T_1 transition, the response is smaller and is anisotropic for the T_2 transition. Below 17 K, up to five of the seven transitions detected in specific heat and magnetization data are also seen in the thermal expansion coefficients [Fig. 1(c)]. The changes in the thermal expansion coefficients through the magnetic transitions are qualitatively similar for both orientations. There are no obvious anomalies in the anisotropic thermal expansion data at and above ~225 K, thus the anomaly detected in resistivity data in this temperature range either is associated with a very broad and subtle structural transition or is some artifact pertinent to transport measurements. Additional studies are required to address this issue.

Anisotropic ambient-pressure resistivity is shown in Fig. 3(a). There are several points of note. The in-plane residual resistivity ratio, $\mathrm{RRR} = \rho(300\ \mathrm{K})/\rho(2\ \mathrm{K}) \approx 10$ in this work, is almost a factor of 2 higher than that in Ref. [9], which suggests better crystallinity or fewer defects and impurities. The structural phase transition T_1 is sharper and ~10 K higher than reported [9]. Moreover, another, hysteretic, possibly structural transition T_2 can be detected in the 85–100 K range. These two transitions are also seen, although somewhat less clearly, in the c-axis resistivity data. There might also be another, very broad and hysteretic, transition above ~225 K [Fig. 3(a)].

At room temperature the anisotropy of resistivity, ρ_c/ρ_{ab}, is about 20 [Fig. 3(b)]. This value changes significantly through the structural and magnetic transitions, thus reflecting the anisotropic contribution of related changes in scattering and

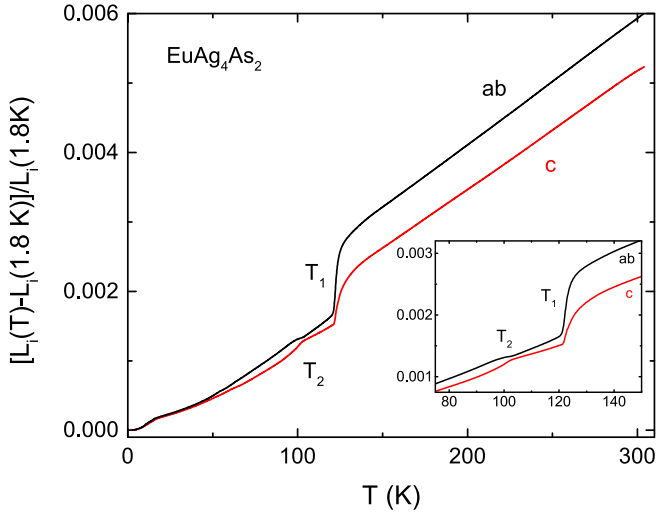

FIG. 2. Anisotropic, normalized to 1.8 K, thermal expansion of $EuAg_4As_2$ measured on warming. Inset: Enlarged region of two structural transitions in anisotropic thermal expansion.

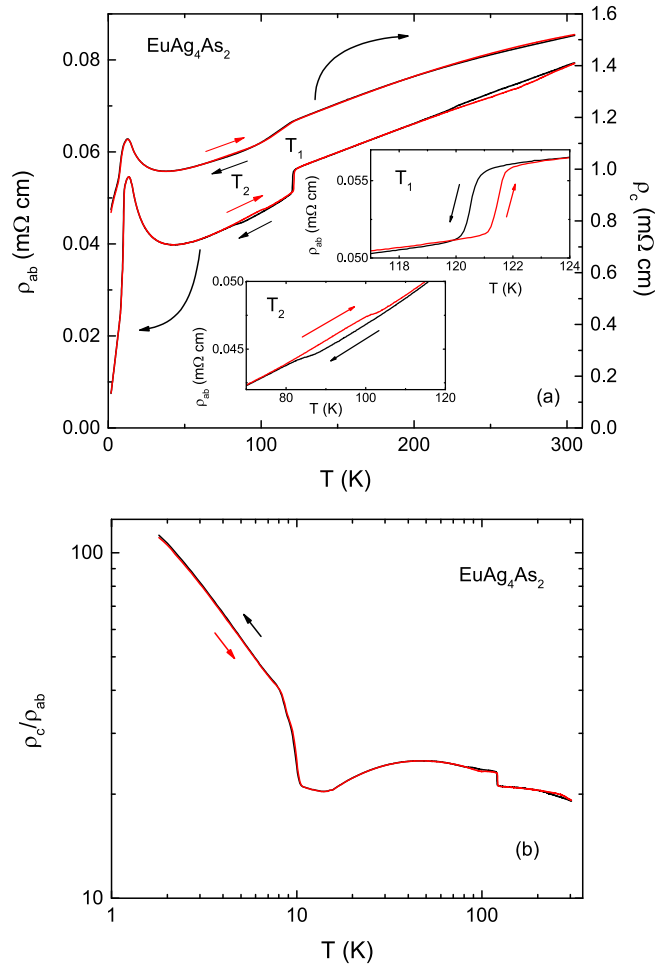

FIG. 3. (a) Anisotropic ambient pressure resistivity of $EuAg_4As_2$ measured on cooling and on warming. Insets: Hystereses of the structural phase transitions as seen in the in-plane resistivity. (b) Resistivity anisotropy of $EuAg_4As_2$ from the data taken on cooling (black line) and on warming (red line).

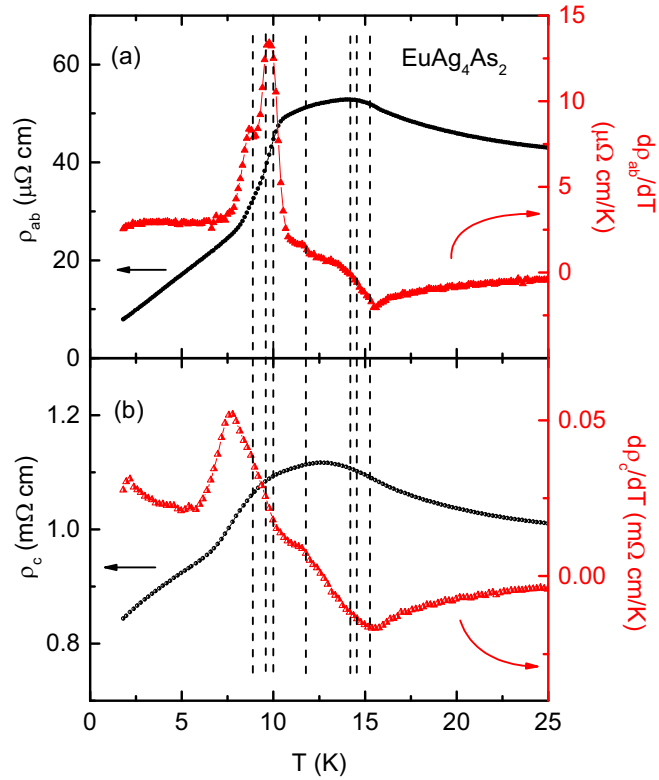

FIG. 4. Low-temperature part of the (a) in-plane and (b) out-of-plane resistivity and their temperature derivatives. Vertical lines mark transitions as seen in the low-temperature heat capacity in Fig. 1(a).

electronic structure to the electronic transport properties. The value of ρ_c/ρ_{ab} reaches $\gtrsim$100 at the base temperature. This may be primarily associated with the large residual resistivity, ρ_0, term (smaller RRR value) found for the ρ_c data. As expected, the behavior of ρ_c/ρ_{ab} is very similar, on the log-log scale, for the data taken on cooling and on warming, with slight differences seen for the T_2 transition and above ~225 K. An ~1 K difference is present in the data for the T_1 transition, even though it is not clearly seen in the large scale log-log plot in Fig. 3(b). Both in-plane and c-axis resistivities have a pronounced upturn above magnetic ordering. This upturn is probably due to scattering on magnetic fluctuations.

The low-temperature part of the in-plane resistivities, ρ_{ab} and ρ_c, together with their respective temperature derivatives, $d\rho_{ab}/dT$ and $d\rho_c/dT$, are shown in Figs. 4(a) and 4(b). There are three clear features in the $d\rho_{ab}/dT$, suggesting three transitions, at 15.5, 9.9, and 8.7 K [24], as well as another, possibly spin reorientation transition, at about 11.7 K. The corresponding feature in $\rho_{ab}(T)$ and its derivative is rather subtle. The out-of-plane resistivity data give the same transition temperatures if, for two lower transitions, a different criterion, the middle point of the increase in $d\rho_c/dT$ [25], is utilized.

Comparison of low-temperature thermodynamic (Fig. 1) and transport (Fig. 4) data leads to several conclusions. The feature in $d\rho_c/dT$ at ~7.5 K does not have its counterpart in any of the thermodynamic measurements presented in Fig. 1 so it does not seem to be related to a thermodynamic phase transition. Although the low-temperature transitions seen in

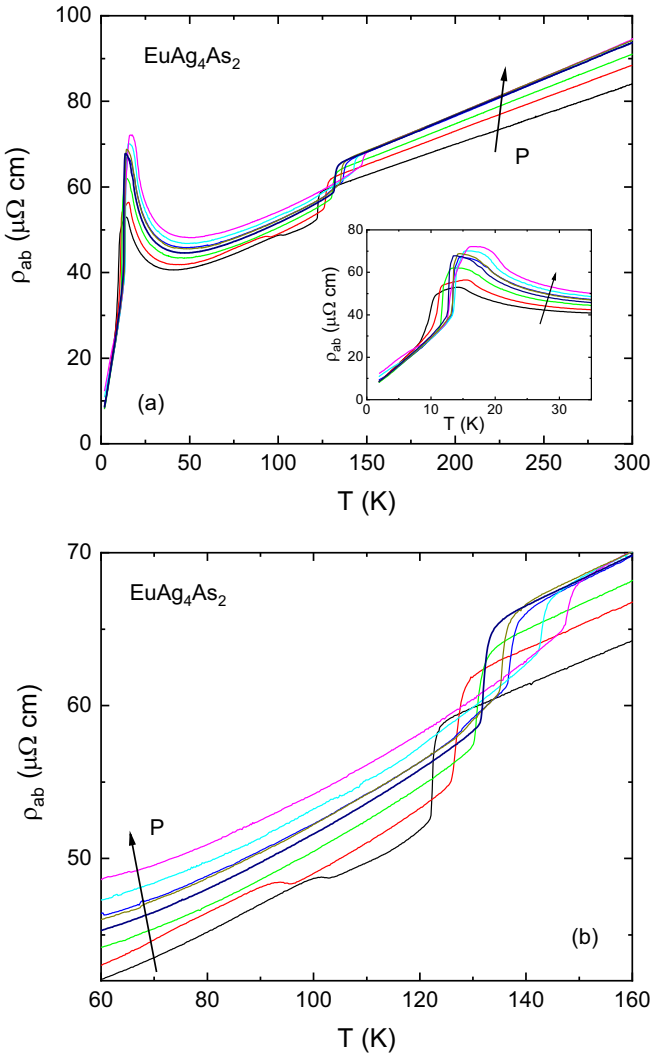

FIG. 5. (a) Temperature-dependent resistivity of $EuAg_4As_2$ measured at different pressures (a subset of the data is shown). Inset: Enlarged region of magnetic transitions. (b) Enlarged region of structural transitions. Arrows show the direction of the pressure increase. The low-temperature values of pressure are 0.02, 4.0, 9.4, 10.5, 13.6, 15.1, 18.2, and 20.8 kbar. Data taken on warming are shown.

$d\rho_{ab}/dT$ are only a subset of the transitions occurring in $EuAg_4As_2$, they do correlate with the primary features and span of the transitions detected and can serve as a caliper of how the magnetism in $EuAg_4As_2$ responds to pressure.

Based on the above, measurements of the in-plane resistivity allow for the tracking of two high-temperature structural transitions as well as of a subset of the low-temperature magnetic transitions. In the following we present the $\rho_{ab}(T)$ measurements under pressure in order to provide an initial mapping of the P-T phase diagram for $EuAg_4As_2$.

B. Resistivity under pressure

The evolution of the in-plane resistivity under pressure up to 20.8 kbar is shown in Fig. 5. With applied pressure, the upper structural transition moves up, as do the lower-temperature, magnetic transitions. The lower structural transition appears to move down under pressure [Fig. 5(b)] and soon becomes undetectable. As the pressure increases, the upturn above the magnetic transitions becomes more pronounced, and away from the phase transition temperatures, the resistivity generally increases too.

The low-temperature resistivities for two representative pressures, 0.02 and 18.2 kbar, are shown in Figs. 6(a) and 6(b), respectively. (Note that the 0.02 kbar data are very close to the ambient-pressure data taken outside the pressure cell, which suggests that for the measurement protocol used the thermal mass of the pressure cell has no significant effect on the size of hysteresis.) At higher pressures the magnetic transitions are sharper and the hysteresis is larger. It should be noted that the upper magnetic transition (T_{M3}) that appears as a single anomaly at low pressures [Fig. 6(c)] appears as two anomalies at higher pressures [Fig. 6(d)], indicating that either it splits under pressure or one of the neighboring, ambient-pressure transitions becomes resolvable as the pressure is increased (Fig. 7). It is curious that apparently the anomaly at T_{M2} is reduced under pressure, whereas the one at T_{M1} is enhanced. Such a change in magnetic scattering causing changes in the relative intensity of resistive anomalies could be related to changes in the magnetic structure under pressure.

Figure 7 presents the pressure dependence of the three magnetic transitions as resolved by in-plane resistivity measurements. The two lower transition temperatures, T_{M1} and T_{M2}, increase under pressure; the higher one, T_{M3}, splits into two (T_{M3} and T_{M3A}) at and above ~7.3 kbar. Whereas T_{M3} and T_{M3A} increase linearly under pressure with the pressure derivatives $dT_{M3}/dP = 0.25$ K/kbar and $dT_{M3A}/dP = 0.28$ K/kbar, for the lower transitions, T_{M1} and T_{M2}, the behavior under pressure is better fit with the second-order polynomial with initial ($P \to 0$) values of the derivatives $dT_{M1}/dP = 0.41$ K/kbar and $dT_{M2}/dP = 0.34$ K/kbar. In a simple model that considers RKKY interactions [26] the pressure dependence of the magnetic ordering temperature depends on the pressure dependencies of two parameters: the density of states and the effective RKKY exchange parameter. The behavior observed in a specific material is the result of competition of these two contributions.

The resistivity minimum that precedes these magnetic transitions (Fig. 8) shifts to higher temperatures under pressure at the rate of 0.42 K/kbar, which is faster than the upper magnetic transition. The size of the resistivity upturn also increases under pressure (Fig. 8). At least in part this is simply due to the increase in the temperature range over which the upturn is observed.

Now we turn to structural phase transitions under pressure. As shown in Figs. 5 and 9, the higher structural transition, T_1, is observed in all pressure ranges in this work. The transition temperature increases under pressure. The behavior clearly changes between two pressure ranges: below ~14 kbar the $T_1(P)$ is linear, with $dT_1/dP \approx 0.9$ K/kbar, whereas above ~14 kbar the pressure derivative changes by a factor of 2, to $dT_1/dP \approx 1.9$ K/kbar. The thermal hysteresis, ~3.3 K is basically pressure independent. The lower structural transition, T_2, initially decreases under pressure at a rate of between −3 and −4 K/kbar. Its signature in $\rho_{ab}(T)$, even at ambient pressure, is rather subtle and we are no longer able to detect it

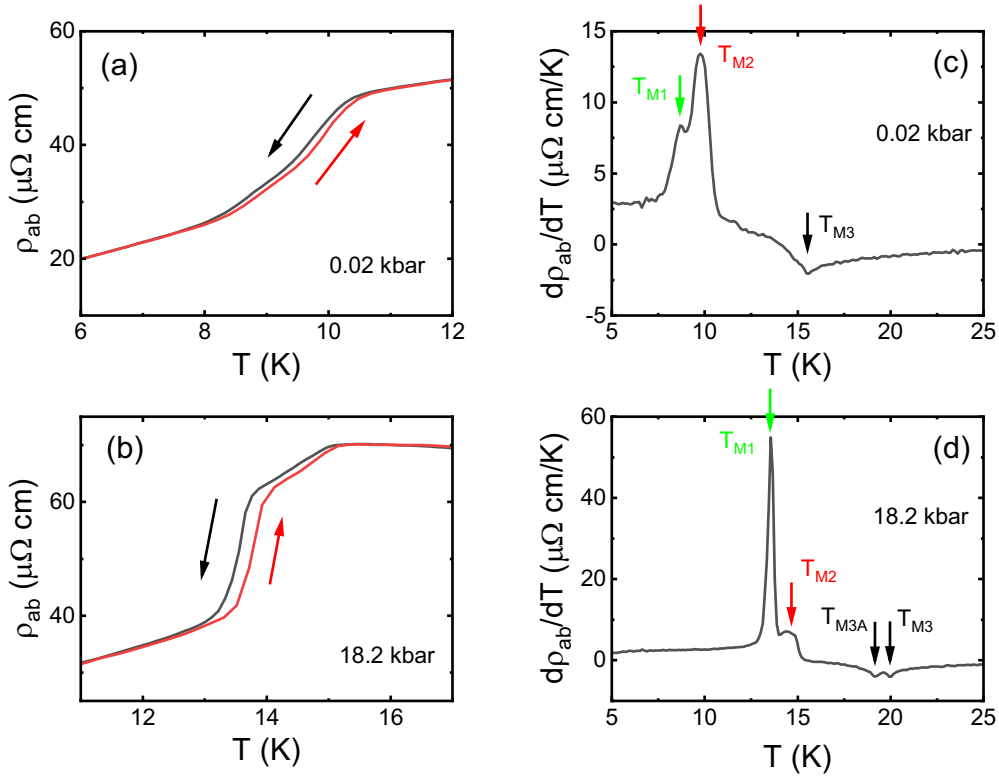

FIG. 6. (a, b) Low-temperature resistivity measured on cooling and warming; (c, d) low-temperature derivatives $d\rho_{ab}/dT$ (for measurements on cooling) at two representative pressures, 0.02 and 18.2 kbar. Arrows mark transitions. Note that the upper transition splits in two under pressure.

at and above ∼7.3 kbar, possibly because of the rather strong, nonmonotonic background.

It is noteworthy that a weak, but discernible, anomaly in the 10–15 kbar range is also observed in pressure dependencies of

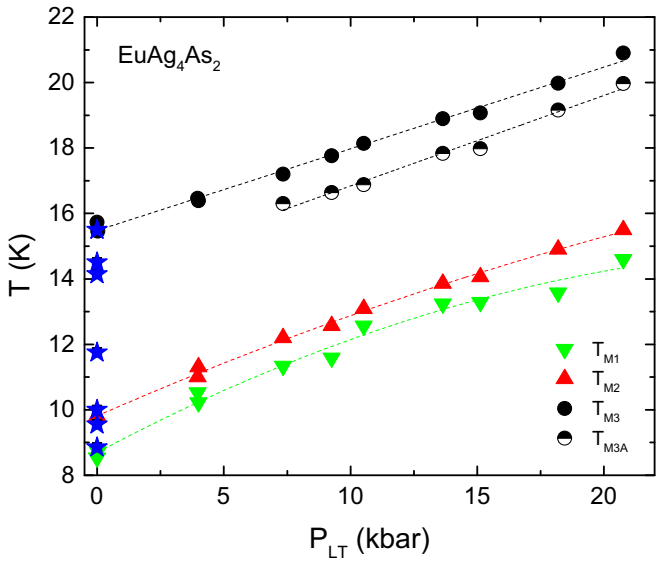

FIG. 7. Pressure dependence of the magnetic ordering temperatures in $EuAg_4As_2$ determined from $\rho_{ab}(T)$ measurements (circles and triangles). Stars: ambient pressure transitions from heat capacity data.

the high- and low-temperature resistivity data, both above and below all noted transition temperatures (Fig. 10).

It has to be mentioned that, as shown in Refs. [14] and [15], the solidification temperatures of the pressure media are pressure dependent. For the particular medium used in this work the solidification temperature at ambient pressure is 120 K and at 30–35 kbar it solidifies at room temperature. The observed anomalies in several quantities do not correspond to crossing of the medium solidification line, so these anomalies are not artifacts of the change in the experimental conditions.

The cause of the anomalies observed in the 10–15 kbar pressure range for several experimental quantities in $EuAg_4Sb_2$ deserves further studies. One of the possible scenarios might be a significant change in the electronic structure under pressure, e.g., via an electronic topological transition (Lifshitz transition) [27] that is not accompanied or caused by a structural transition but still would affect electronic properties.

Finally, we can analyze the change in the jump in resistivity at the upper structural transition as a function of the pressure (Fig. 11). Its value decreases under pressure with linear extrapolation to $\Delta\rho_{s1} = 0$ at ∼32.5 kbar, which would correspond to the (extrapolated) value of $T_1 \sim 165$–170 K. There are several possible scenarios of what might happen above ∼32.5 kbar. Probably, the structural transition will continue to exist with the transition temperature increasing further under pressure, however, either without the discernible feature in ρ_{ab} or with inversion of this feature (decrease in ρ_{ab} at T_1 on warming).

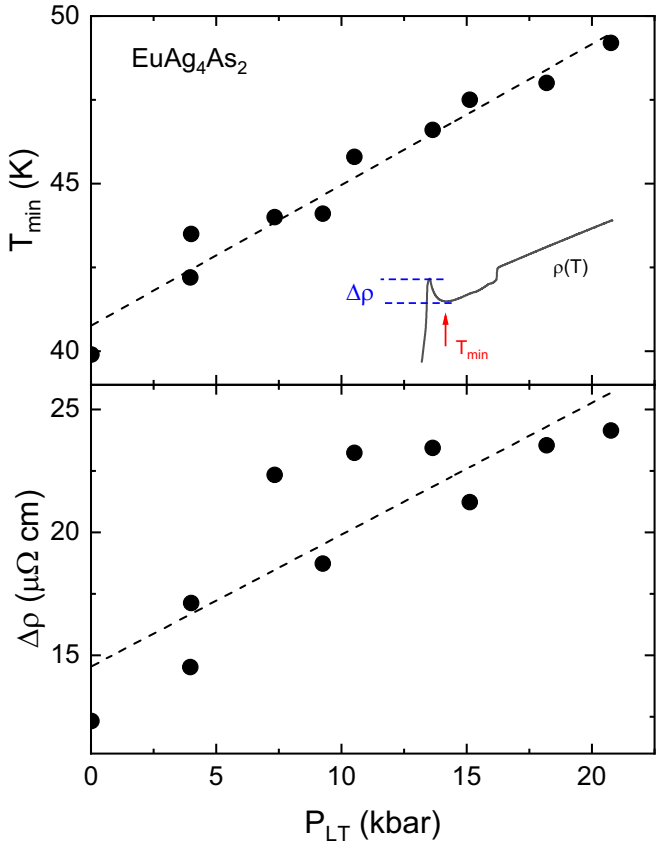

FIG. 8. Pressure dependence of the temperature of the resistivity minimum, T_{min} (top panel), and the size of the resistivity upturn, $\Delta\rho$ (bottom panel), for the in-plane resistivity of $EuAg_4As_2$. Dashed lines are linear fits to the data. The definitions of T_{min} and $\Delta\rho$ are shown in the top panel.

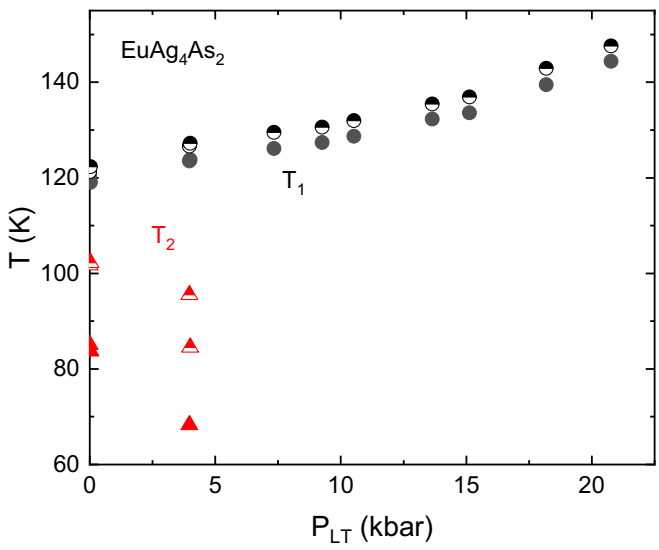

FIG. 9. Pressure dependence of the structural transition temperatures, T_1 and T_2. Filled symbols, measured on cooling; half-filled symbols, measured on warming. Data at $P \approx 4.0$ kbar were taken twice: on an increase in and a release of pressure.

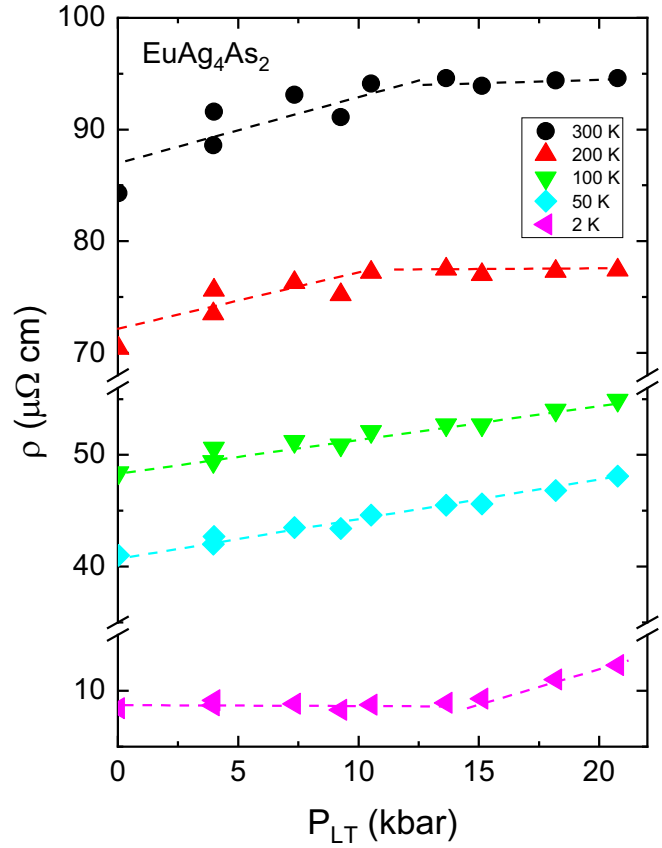

FIG. 10. Pressure dependence of the in-plane resistivity of $EuAg_4As_2$ at selected temperatures. Dashed lines are guides for the eye.

IV. DISCUSSION AND SUMMARY

Our resistivity measurements under pressure as well as ambient-pressure thermodynamic and transport measure-

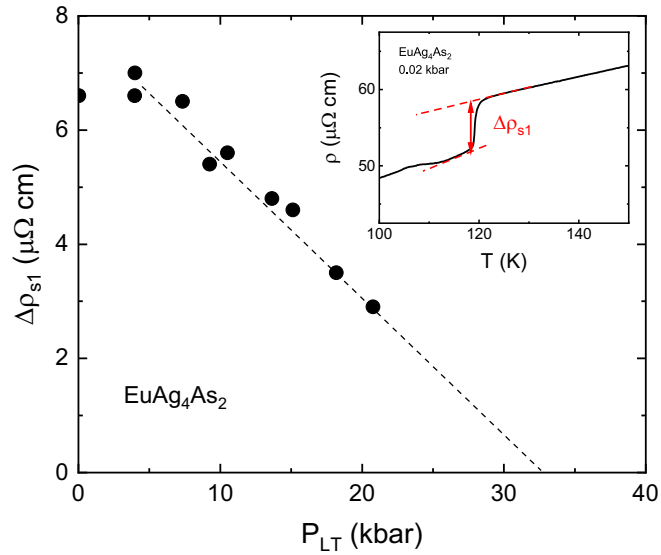

FIG. 11. Pressure dependence of the size of the resistivity upturn, $\Delta\rho_{s1}$, at the higher structural transition, T_1. Inset: Definition of $\Delta\rho_{s1}$.

ments further underscore the complexity of $EuAg_4As_2$ as a host for a multitude of structural and magnetic phases. In addition to documenting the evolution of different phases under pressure this work provides a roadmap for further studies, if undertaken.

The signs of the initial pressure derivatives of the structural and magnetic phase transitions are consistent with those inferred from the combination of the specific heat data and the thermal expansion data in this work via Clausius-Clapeyron (first-order phase transitions) or Ehrenfest (second-order phase transitions) relations [28]. It is curious, though, that given the anisotropic, trigonal structure of $EuAg_4As_2$, its in-plane and c-axis thermal expansion evolution is similar for the higher structural (T_1) and all three magnetic transitions, and only at the lower structural transition T_2 are different signs of thermal expansion observed (Fig. 2).

The resistivity of $EuAg_4As_2$ over wide temperature ranges increases under pressure, suggesting either a pressure-induced decrease in the density of states at the Fermi level or a decrease in mobility (increase in effective mass). Note that for the related compound, $SrAg_4As_2$, the opposite trend, a decrease in the in-plane resistivity under pressure, was reported [11].

The magnetic transitions shift to higher temperatures under pressure. The values of the pressure derivatives are rather conventional.

A better understanding of the nature of the lower structural transition, T_2, and its evolution under pressure above ∼4 kbar would require careful scattering studies. It is of interest, assuming that this transition can be suppressed down to $T = 0$ K, whether it has, even subtle, effects on the magnetic transitions.

The upper structural transition temperature, T_1, increases under pressure with a kink in $T_1(P)$ at ∼14 kbar, whereas the jump in ρ_{ab} associated with it gets smaller. Linear extrapolation suggests that the jump will disappear at 30–35 kbar. This behavior is very different from that of the structural transition in $SrAg_4As_2$ [11], which has a minimum at ∼7.5 kbar both in $T_s(P)$ and in $\Delta\rho_{xx}(P)$. Further studies are required to understand what will happen with the upper structural transition and its signature in the in-plane resistivity and, broadly speaking, to the electronic structure, above ∼32.5 kbar.

The anomaly in the higher-temperature, structural phase transition, $T_1(P)$, behavior in the 10–15 kbar range is also present in the $\rho(P)$ data both above and below all noted transition temperatures. Are these anomalies associated with changes in the electronic structure? and What is the origin of these changes? These questions will require further studies. Additionally, some understanding of the nature of the differences in the pressure responses of $EuAg_4As_2$ and $SrAg_4As_2$ would be desirable.

ACKNOWLEDGMENTS

The authors thank Dominic Ryan and Elena Gati for useful discussions. Work at the Ames Laboratory was supported by the U.S. Department of Energy, Office of Science, Basic Energy Sciences, Materials Sciences and Engineering Division. The Ames Laboratory is operated for the U.S. Department of Energy by Iowa State University under Contract No. DE-AC02-07CH11358. L.X. was supported, in part, by the W. M. Keck Foundation. Work at UCLA was supported by the U.S. Department of Energy, Office of Science, Office of Basic Energy Sciences, under Award No. DE-SC0011978.

[1] Y. Kamihara, H. Hiramatsu, M. Hirano, R. Kawamura, H. Yanagi, T. Kamiya, and H. Hosono, J. Am. Chem. Soc. **128**, 10012 (2006).
[2] Y. Kamihara, T. Watanabe, M. Hirano, and H. Hosono, J. Am. Chem. Soc. **130**, 3296 (2008).
[3] G. R. Stewart, Rev. Mod. Phys. **83**, 1589 (2011).
[4] A. Chubukov and P. J. Hirschfeld, Phys. Today **68**(6), 46 (2015).
[5] S. Zapf and M. Dressel, Rep. Prog. Phys. **80**, 016501 (2017).
[6] A. E. Böhmer and A. Kreisel, J. Phys.: Condens. Matter **30**, 023001 (2017).
[7] S. S. Stoyko, M. Khatun, C. S. Mullen, and A. Mar, J. Solid State Chem. **192**, 325 (2012).
[8] B. Gerke, C. Schwickert, S. S. Stoyko, M. Khatun, A. Mar, and R. Pöttgen, Solid State Sci. **20**, 65 (2013).
[9] B. Shen, C. Hu, H. Cao, X. Gui, E. Emmanouilidou, W. Xie, and N. Ni, arXiv:1809.07317.
[10] D. H. Ryan, S. L. Bud'ko, C. Hu, and N. Ni, AIP Adv. **9**, 125050 (2019).
[11] B. Shen, E. Emmanouilidou, X. Deng, A. McCollam, J. Xing, G. Kotliar, A. I. Coldea, and N. Ni, Phys. Rev. B **98**, 235130 (2018).
[12] G. M. Schmiedeshoff, A. W. Lounsbury, D. J. Luna, S. J. Tracy, A. J. Schramm, S. W. Tozer, V. F. Correa, S. T. Hannahs, T. P. Murphy, E. C. Palm, A. H. Lacerda, S. L. Bud'ko, P. C. Canfield, J. L. Smith, J. C. Lashley, and J. C. Cooley, Rev. Sci. Instrum. **77**, 123907 (2006).
[13] S. L. Bud'ko, A. N. Voronovskii, A. G. Gapotchenko, and E. S. ltskevich, Zh. Eksp. Teor. Fiz. **86**, 778 (1984) [Sov. Phys. JETP **59**, 454 (1984)].
[14] S. K. Kim, M. S. Torikachvili, E. Colombier, A. Thaler, S. L. Bud'ko, and P. C. Canfield, Phys. Rev. B **84**, 134525 (2011).
[15] M. S. Torikachvili, S. K. Kim, E. Colombier, S. L. Bud'ko, and P. C. Canfield, Rev. Sci. Instrum. **86**, 123904 (2015).
[16] A. Eiling and J. S. Schilling, J. Phys. F: Met. Phys. **11**, 623 (1981).
[17] E. S. Itskevich, Cryogenics, **4**, 365 (1964).
[18] E. S. Itskevich, A. N. Voronovskii, A. F. Gavrilov, and V. A. Sukhaparov, Cryogenics **7**, 359 (1967).
[19] W. M. Becker, K. Hoo, and P. G. Winchell, Rev. Sci. Instrum. **47**, 587 (1976).
[20] H. Fujiwara, H. Kadomatsu, and K. Tohma, Rev. Sci. Instrum. **51**, 1345 (1980).
[21] J. D. Thompson, Rev. Sci. Instrum. **55**, 231 (1984).
[22] M. E. Fisher, Philos. Mag. **7**, 1731 (1962).
[23] T. A. Wiener and P. C. Canfield, J. Alloys Compd. **303-304**, 505 (2000).
[24] M. E. Fisher and J. S. Langer, Phys. Rev. Lett. **20**, 665 (1968).

[25] V. Taufour, U. S. Kaluarachchi, R. Khasanov, M. C. Nguyen, Z. Guguchia, P. K. Biswas, P. Bonfà, R. De Renzi, X. Lin, S. K. Kim, E. D. Mun, H. Kim, Y. Furukawa, C.-Z. Wang, K.-M. Ho, S. L. Bud'ko, and P. C. Canfield, Phys. Rev. Lett. **117**, 037207 (2016).

[26] J. S. Schilling, Adv. Phys. **28**, 657 (1979).

[27] I. M. Lifshitz, ZhETF **38**, 1569 (1960); JETP **11**, 1130 (1960) (in English).

[28] T. H. K. Barron and G. K. White, *Heat Capacity and Thermal Expansion at Low Temperatures* (Kluwer, New York, 1999).